Reaction Chemistry & Engineering

ROYAL SOCIETY OF CHEMISTRY

PAPER

View Article Online
View Journal | View Issue

Cite this: *React. Chem. Eng.*, 2024, **9**, 654

A novel diamine non-aqueous absorbent based on *N*-methyl diethanolamine regulation for energy-efficient CO_2 capture†

Zhen Wang,[a] Zhitao Han, *[a] Xiao Yang,[a] Zelu Zhou,[a] Xi Wu,[a] Song Zhou[b] and Shijian Lu[c]

Non-aqueous absorbents receive more and more attention due to their low sensible heat and evaporation latent heat. But their low CO_2 desorption efficiency and high desorption reaction heat are still major limits for practical application. Herein, a novel non-aqueous diamine absorbent based on alkanolamine regulation is proposed. In the experiments, monoethanolamine (MEA) was used as the main absorbent for ensuring high CO_2 absorption capacity and absorption rate, while polyethylene glycol 200 (PEG200) was used as a cosolvent to reduce evaporation latent heat. Subsequently, MEA/PEG200 non-aqueous absorbents were composed with three typical secondary/tertiary amines including *N*-methyldiethanolamine (MDEA), diethanolamine (DEA) and triethanolamine (TEA), respectively, and their regulation effects on CO_2 capture performance were investigated systematically. The results showed that the MEA/MDEA/PEG non-aqueous system exhibited a superior CO_2 desorption performance. The corresponding maximum regeneration efficiency reached up to 82.1%, which was significantly higher than the case without addition of MDEA. It still kept a high CO_2 desorption efficiency (79%) after the 8th regeneration cycle. According to thermodynamic analysis, the desorption reaction heat for the MEA/MDEA/PEG non-aqueous system was only 1.40 GJ per ton CO_2, which was 20% lower than the non-aqueous MEA/PEG200 absorbent. And its total regeneration energy consumption was 1.90 GJ per ton CO_2, which was reduced by 48.1% compared to MEA aqueous solution. FT-IR, ^{13}C-NMR and DFT calculations indicated that the introduction of the MDEA regulator would result in a much lower reaction energy barrier between zwitterions and MDEA compared to that between zwitterions and MEA. Besides, it would induce the formation of protonated MDEA ($MDEAH^+$), which was much easier for MDEA regeneration.

Received 26th September 2023,
Accepted 28th November 2023

DOI: 10.1039/d3re00506b

rsc.li/reaction-engineering

1. Introduction

It is known that global CO_2 emission in 2021 is estimated to be 34.9 billion tons. Such a great deal of CO_2 emission will undoubtedly contribute to an obvious greenhouse effect.[1,2] Over the past decades, more and more strategies have been proposed to control CO_2 emission. CO_2 capture and storage (CCS) is considered as one of the most promising techniques.[3,4] Among the developed CCS methods, chemical absorption is considered to be the most feasible one for stationary and mobile sources. And amine-based absorbents have been widely used in many demonstration projects because of their high CO_2 capture capacity and good applicability. But they still face some challenges, especially the high energy consumption in the CO_2 desorption process, which limits the scale application of CCS techniques in industrial areas to a large extent.[5,6] For example, the representative monoethanolamine (MEA) aqueous solution requires a large amount of energy during regeneration due to the high specific heat capacity and high vapor pressure of water. It leads to a high level of regeneration energy consumption (3.2–4.0 GJ per ton CO_2), accounting for 70–80% of overall CCS operating costs.[7–10] Therefore, it is imperative to develop novel CO_2 absorbents to reduce energy consumption in the CO_2 desorption process.

[a] *Marine Engineering College, Dalian Maritime University, No.1, Linghai Road, Dalian 116026, China. E-mail: hanzt@dlmu.edu.cn; Tel: +86 138 9869 2035*
[b] *Power and Energy Engineering College, Harbin Engineering University, Harbin 150001, China*
[c] *Carbon Neutral Institute, China University of Mining and Technology, Xuzhou 221008, China*

† Electronic supplementary information (ESI) available: Schematic diagram of the CO_2 desorption setup (Fig. S1); different MEA/MDEA/PEG200 non-aqueous absorbent systems (Table S1); cyclic CO_2 absorption–desorption capacity of the MEA/MDEA/PEG200 system (Fig. S2); vapor–liquid equilibrium (VLE) data of different absorbents (Fig. S3); CO_2 absorption and desorption performance of the 30M/P system (Fig. S4); comparison of the viscosity of different non-aqueous absorbents (Table S2); physicochemical properties of various components (Table S3); the mass of the absorbent, desorbed CO_2 and absorbent loss during regeneration (Table S4). See DOI: **https://doi.org/10.1039/d3re00506b**

The regeneration energy consumption (Q_{reg}) is mainly composed of desorption reaction heat (Q_{rea}), sensible heat (Q_{sen}) and evaporation latent heat (Q_{lat}).[11] After the CO_2 absorption process is completed, the CO_2-rich liquid is thermally decomposed in the regeneration tower to release CO_2, and the energy required for the regeneration process is derived from the waste heat of power plants, which is supplied by a reboiler at the bottom of the regeneration tower. As for organic amine aqueous solutions, the heating and evaporation of water requires significant energy consumption during CO_2 desorption. In view of this, developing CO_2 absorbents with a low sensible and evaporative sensible heat is crucial to achieve low energy consumption. Non-aqueous absorbents have attracted increasing attention in recent years. It is due to the fact that they can use organic solvents with low specific heat capacity and low vapor pressure to replace water, which greatly reduces the energy requirement for heating and evaporation of solution.[12,13] Commonly, non-aqueous absorbents include ionic liquids, phase change absorbents and homogeneous absorbents.[14–16] Among them, ionic liquids are recognized as environmentally friendly absorbents because of their low corrosivity, volatility and degradability.[17] But ionic liquids usually possess high viscosity, which is detrimental to overall mass transfer, thus resulting in a relatively lower CO_2 absorption capacity compared to organic amine absorbents.[18–20] During the CO_2 capture process, both CO_2-rich and CO_2-poor phases will be formed in phase change absorbents. The energy consumption for CO_2 desorption can be significantly reduced because only the CO_2-rich phase needs to be sent to the stripper for regeneration. According to the split phase characteristics of phase change absorbents, the viscosity of the CO_2-rich concentrated phase is much higher than that of the CO_2-poor phase. When considering the complexity of a practical flue gas scenario, it may be very difficult to achieve a satisfactory phase separation effect. The viscous CO_2-rich phase is liable to cause pipeline blockage.[21–25]

As for homogeneous non-aqueous absorbents, they are usually made of amines, organic alcohols and their derivatives. Since the specific heat capacity and vapor pressure of organic alcohols are much lower than those of water, it is conducive to greatly reducing the sensible heat and evaporation latent heat during CO_2 desorption. Meanwhile, the hydroxyl groups in organic alcohols have a strong affinity for CO_2, which is also helpful for improving CO_2 capture capacity.[26–31] In this regard, homogeneous non-aqueous absorbents have been considered as one of the most promising absorbents in recent years. Qi *et al.* investigated the thermal stability from 300 K to 700 K as well as the viscosity and VLE data from 298.15 K to 353.15 K of different alkanolamine and PEG200 mixed absorbents.[32] Yu *et al.* reported that the replacement of H_2O with methanol could significantly reduce the sensible heat of the MEA system, resulting in a 24% reduction of overall regeneration energy consumption.[33] Guo *et al.* proposed a homogeneous non-aqueous absorbent made of MEA and glycol ether 2-methoxyethanol (2ME), which could significantly reduce regeneration energy consumption by about 55% as compared to the aqueous 5.0 M MEA system.[34] Though these non-aqueous absorbents can obviously reduce the sensible heat and evaporation latent heat, they still have a low CO_2 desorption efficiency and a high desorption reaction heat. And the desorption reaction heat is mainly determined by amine species in the absorbent regeneration process. Since non-aqueous absorbents typically use primary amines with a high CO_2 absorption rate and capacity as main absorbents, which react with CO_2 to form a product with high thermal stability, a significant increase in desorption reaction heat is observed. Previous studies indicate that primary amine (RNH_2) can react with CO_2 through a zwitterion mechanism: firstly, RNH_2 reacts with CO_2 to generate zwitterions (RNH_2^+-COO^-), which then further react with RNH_2 to form carbamates (RNH^+COO^-) and protonated amines (RNH_3^+).[35–37] The desorption reaction heat mainly corresponds to the energy for breaking C–N and C–O bonds in carbamates and deprotonating protonated amines.[38] Since both primary amine carbamates and protonated amines have a high activation energy barrier, it will lead to a greater desorption reaction heat and a lower CO_2 desorption efficiency for non-aqueous absorbents.

$$CO_2 + RNH_2 \Leftrightarrow RNH_2^+COO^- \quad (1)$$

$$RNH_2^+COO^- + RNH_2 \Leftrightarrow RNH^+COO^- + RNH_3^+ \quad (2)$$

It is known that secondary amine (R_2NH) reacts with CO_2 to generate secondary carbamates ($R_1NR_2COO^-$) and protonated amines ($R_1R_2NH_2^+$) while tertiary amine (R_3N) reacts with CO_2 to generate carbonates (CO_3^{2-}/HCO_3^-) and tertiary protonated amines ($R_1R_2R_3NH^+$). Though both R_2NH and R_3N have a relatively lower CO_2 absorption capacity compared to primary amines, their products possess lower thermal stability and are more susceptible to decomposition due to the steric hindrance effect of alkyl groups connected to the N atom.[39,40] Zhou *et al.* reported that the introduction of sterically-hindered amines in the absorbent resulted in a significant decrease of desorption reaction heat.[41,42] Shi *et al.* reported that the desorption reaction heat could be drastically reduced by manipulating proton transfer from strongly basic RNH_2 to moderately basic R_2NH or weakly basic R_3N.[43,44] The results demonstrate that the introduction of secondary/tertiary amine as a regulator in non-aqueous absorbents may change the proton transfer pathway between the primary amine and CO_2, generating carbamates and protonated amines with a low-energy barrier, thus achieving a lower reaction heat and a higher desorption efficiency in the CO_2 desorption process. But to the best of our knowledge, the research on the introduction of secondary/tertiary amine as a regulator into primary amine-based non-aqueous absorbents is still lacking. Therefore, it is interesting to systematically explore the regulation effects of secondary/

tertiary amine on CO_2 desorption performance of traditional primary amine-based absorbents with the aim to develop a novel non-aqueous CO_2 absorbent for high-efficiency and energy-saving CO_2 capture.

In this paper, the low-cost MEA with a high CO_2 absorption capacity and absorption rate was selected as the main CO_2 absorbent. The non-toxic organic solvent PEG200 is used as a cosolvent due to its lower specific heat capacity and vapor pressure compared to water.[45,46] Different secondary/tertiary amines such as *N*-methyldiethanolamine (MDEA), diethanolamine (DEA) and triethanolamine (TEA) were added to the MEA/PEG200 non-aqueous absorbent as regulators to screen the diamine non-aqueous system with better CO_2 desorption performance. Based on these results, the effect of different concentrations of components in diamine non-aqueous absorbents on CO_2 capture performance was further investigated. In addition, the effects of different desorption temperatures on the solvent regeneration performance and the long-term stability of the diamine nonaqueous absorbents were also evaluated. Finally, the thermodynamics of the diamine non-aqueous absorbents was analyzed and the reaction mechanism in the CO_2 capture process was elucidated using FTIR, ^{13}C-NMR and DFT calculations.

2. Experimental

2.1 Chemicals and materials

MEA (99%), MDEA (99%), DEA (99%), and TEA (99%) were purchased from Aladdin Reagent Shanghai Co., Ltd. PEG200 (99%) was provided by Sinopharm Chemical Reagent Co., Ltd. Pure CO_2 (99.999%) and N_2 (99.999%) were obtained from Dalian Special Gases Co., Ltd. The physical and chemical property data of selected reagents are summarized in Table S3.† All chemicals in this study were used without further purification.

2.2 CO_2 absorption and desorption

The absorption experiments were conducted based on a customized CO_2 absorption system, as shown in Fig. 1. The mass of the non-aqueous absorbent was kept at 50 g and total organic amine concentrations were maintained constant at 30 wt%. Before the CO_2 absorption experiment was started, the entire system was purged with N_2 to remove air. After that, the prepared CO_2 absorbent was heated to 313 ± 1 K in a water bath (Julabo, German). Lastly, a feed gas consisting of 90% N_2 and 10% CO_2 was blown into the solution at a constant flow rate of 1.2 L min^{-1} by adjusting the mass flow meters (Sevenstar, China). The inlet and outlet gas concentrations were measured with a gas analyzer (MRU, German). When the CO_2 outlet concentration approached the CO_2 inlet concentration, it was considered that the non-aqueous absorbent reached saturation. The instantaneous CO_2 absorption rate (r_{abs}, mol min^{-1}) and accumulative CO_2 absorption amount (n_{abs}, mol kg^{-1}) were defined as follows:

$$r_{abs} = \frac{1.2 \times (C_{Ain} - C_{Aout})}{22.4} \quad (3)$$

$$n_{abs} = \frac{1.2 \times \int_0^t (C_{Ain} - C_{Aout}) dt}{22.4} \quad (4)$$

where C_{Ain} (L min^{-1}) and C_{Aout} (L min^{-1}) represent the initial CO_2 concentration in the feeding gas and the instantaneous CO_2 concentration in the outlet gas, respectively.

The experimental setup for CO_2 desorption is shown in Fig. S1.† In the CO_2 desorption process, the CO_2-saturated solution was transferred to a three-neck flask, and the temperature of the non-aqueous absorbent was controlled by heating in an oil

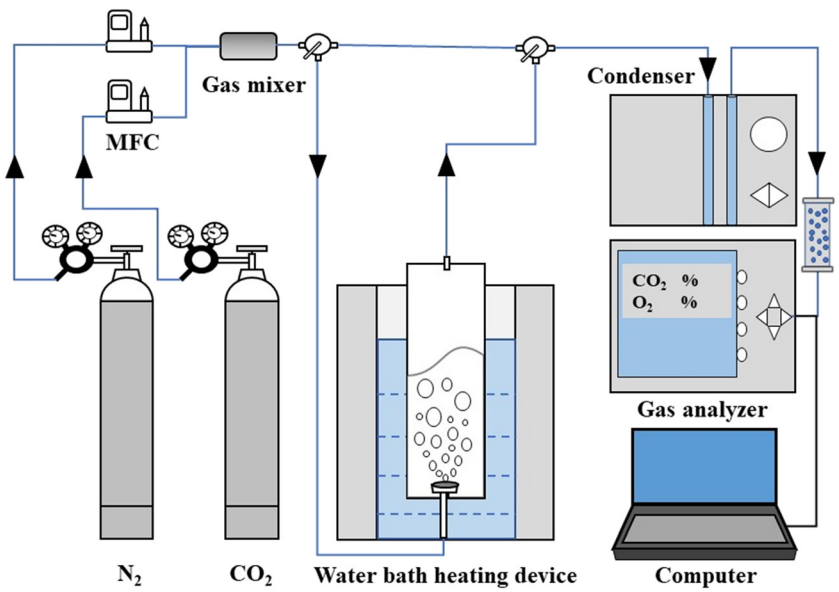

Fig. 1 Schematic diagram of the CO_2-absorption apparatus.

bath. A N_2 stream with a flow rate of 0.2 L min^{-1} was bubbled in the saturated solution. Since the gas analyzer required a steady sampling rate of 1 L min^{-1}, the outlet gas from the bubble reactor was mixed with a second N_2 stream with a flow rate of 1 L min^{-1}. When the measured CO_2 concentration was below 0.5% for 5 minutes, each test was ended. After the desorption experiment, the regenerated solution was cooled to room temperature for the next cycle of CO_2 absorption experiment. CO_2 desorption efficiency (η_{des}, %) was defined as the ratio of CO_2 desorption capacity (n_{des}, mol kg^{-1}) to CO_2 absorption capacity (n_{abs}, mol kg^{-1}) during the absorbent regeneration process. The instantaneous CO_2 desorption rate (r_{des}, mol min^{-1}) and accumulative CO_2 desorption amount (n_{des}, mol kg^{-1}) were calculated through eqn (6) and (7), respectively.

$$\eta_{des} = \frac{n_{des}}{n_{abs}} \times 100\% \quad (5)$$

$$r_{des} = \frac{1.2 \times C_{Dout}}{22.4} \quad (6)$$

$$n_{des} = \frac{1.2 \times \int_0^t C_{Dout} dt}{22.4} \quad (7)$$

where C_{Dout} represents the instantaneous CO_2 concentration in purged gas.

All CO_2 absorption–desorption experiments in this paper were repeated three times to ensure the reliability of experimental data.

2.3 Regeneration heat duty

The regenerative heat duty (Q_{reg}, GJ t^{-1} CO_2) was mainly composed of desorption reaction heat (Q_{rea}), sensible heat (Q_{sen}) and latent heat (Q_{lat}). The regenerative heat duty was calculated by following eqn (8).

$$Q_{reg} = Q_{rea} + Q_{sen} + Q_{lat} \quad (8)$$

Q_{rea} could be obtained by plotting $\ln P_{CO_2}$ *versus* $1/T$:

$$Q_{rea} = \frac{\partial \ln P_{CO_2}}{\partial(1/T)} \cdot (-R) \quad (9)$$

Q_{sen} represented the energy consumed to heat CO_2-rich solutions from the absorption temperature to the desorption temperature and could be described by eqn (10)–(12).

$$Q_{sen} = \frac{C_p \times m_{sol} \times \Delta T}{m_{CO_2}} \quad (10)$$

$$C_p = \sum_i^n \frac{C_p^i m_i}{m_{sol}} \quad (11)$$

$$m_{CO_2} = \Delta R \times m_{sol} \times M_{CO_2} \quad (12)$$

Q_{lat} was related to evaporation loss of the non-aqueous absorbent in the high temperature regeneration process, which could be calculated using the following equation (eqn (13)).

$$Q_{lat} = \frac{m_{sol}^{vap}}{m_{CO_2}} \Delta H_{sol}^{vap} \quad (13)$$

The values of Q_{rea}, Q_{sen} and Q_{lat} could be calculated according to the above equations and the definitions of relevant symbols in equations are shown in Table 1. The physicochemical properties of various components required for the calculation are listed in the ESI.†

2.4 Characterization

In order to investigate the CO_2 capture mechanism of the non-aqueous absorbent, the infrared spectra of scrubbing solutions after CO_2 absorption and desorption were measured using attenuated total internal reflectance Fourier transform infrared spectra (ATR-FTIR, Nicolet iS 50, USA). The wave number range and resolution in transmission mode were set to 600–4000 cm^{-1} and 4 cm^{-1}, respectively. The reaction products formed during CO_2 capture by non-aqueous absorbents were qualitatively analyzed by ^{13}C NMR (Bruker AVANCE III, Germany). D_2O was chosen as the deuterium reagent and tetramethylsilane (TMS) was used as the internal standard in the test. The ^{13}C spectra of non-aqueous absorbent samples were tested at a magnetic field intensity of 400 MHz.

Table 1 Definitions of symbols used in equations

Symbol	Unit	Definition
P_{CO_2}	kPa	The partial pressure of CO_2 over a solution with the CO_2 loading at a certain temperature
R	J mol^{-1} K^{-1}	Molar gas constant
C_p	kJ K^{-1} kg^{-1}	Specific heat capacity of total non-aqueous absorbent
C_P^i	kJ K^{-1} kg^{-1}	Specific heat capacity of each component
m_{sol}	kg	The mass of regenerated absorbent
m_{CO_2}	kg	The mass of desorbed CO_2
M_{CO_2}	g mol^{-1}	CO_2 molecular weight
ΔR	mol kg^{-1}	CO_2 absorption capacity
ΔT	K	Temperature difference between rich and lean solution, set at 10 K
m_{sol}^{vap}	kg	The mass of absorbent loss during desorption
ΔH_{sol}^{vap}	kJ mol^{-1}	Solution evaporation enthalpy at desorption temperature

The viscosities of different non-aqueous absorbents were measured using a digital rotational viscometer (NDJ-5S, Shanghai Bangxi Instrument Technology Co., Ltd.), and the specific results are shown in Table S2.†

2.5 Density functional theory (DFT)

DFT was used to calculate the energy potential of each component of the non-aqueous absorbent for possible reaction paths with CO_2. According to Grimme's scheme, the dispersion correction of Beck–Lee–Yang–Parr (B3LYP) levels with D3 was integrated and all geometric structures obtained were optimized using a basis set of 6-31G (d, p). And the energy minimum of the structure was verified by vibrational frequency. The activation energy potential was defined as follows:

$$E_a = E_{\text{transition state}} - E_{\text{reactant}} \quad (14)$$

$$\Delta E_{\text{product}} = E_{\text{product}} - E_{\text{reactant}} \quad (15)$$

where E (kJ mol^{-1}) is the minimum energy of the optimized structure; E_{reactant}, $E_{\text{transition state}}$ and E_{product} represent the energies of reactants, transition states and products, respectively.

3. Results and discussion

3.1 Selection of the regulator

For further improving the CO_2 capture performance of the MEA/PEG200 system, three typical alkanolamines including one secondary amine (DEA) and two tertiary amines (MDEA and TEA) were chosen as regulators to integrate with MEA/PEG200 non-aqueous absorbents. In each test, the total amine concentration was kept constant at 30 wt%. When introducing the regulator, its concentration was set at 5 wt%. The non-aqueous absorbent concentrations are listed in Table 2.

The CO_2 absorption and desorption performance of these non-aqueous absorbents were investigated, and the result is shown in Fig. 2. Compared with 30M/P (2.38 mol kg^{-1}), the CO_2 absorption capacity of diamine non-aqueous absorbents decreased to varying degrees when a portion of MEA was substituted by the regulators. Despite all this, the CO_2 absorption capacities of 20M5D/P, 20M5M/P, and 20M5T/P systems could still reach 2.14, 1.98, and 1.96 mol kg^{-1}, respectively. For the 25M5D/P system, due to the relatively high viscosity of DEA, the MEA/PEG200 solution regulated by

Table 2 Different non-aqueous absorbent systems

No.	Solvent	Abbreviation
1	30 wt% MEA, 70 wt% PEG200	30M/P
2	25 wt% MEA, 5 wt% DEA, 70 wt% PEG200	25M5D/P
3	25 wt% MEA, 5 wt% MDEA, 70 wt% PEG200	25M5M/P
4	25 wt% MEA, 5 wt% TEA, 70 wt% PEG200	25M5T/P

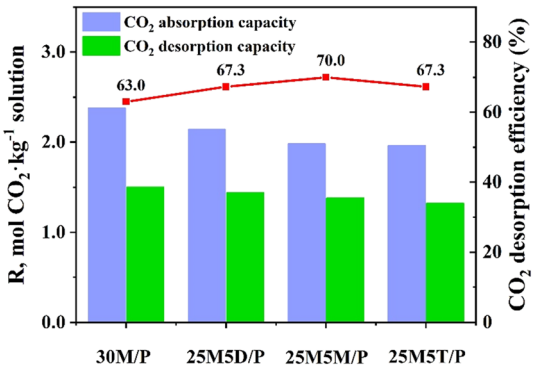

Fig. 2 CO_2 absorption and desorption performance of different non-aqueous absorbents (V_L = 0.05 kg, C_{total} = 30 wt%, $T_{absorption}$ = 313 K, $T_{desorption}$ = 373 K).

DEA exhibited the highest viscosity after CO_2 absorption. It was unfavorable to the gas–liquid mass transfer efficiency, thus leading to a decrease in CO_2 absorption capacity. Likewise, as MDEA and TEA were tertiary amines, they showed very limited ability to react with CO_2 in the absence of water, which also resulted in a reduced CO_2 absorption capacity. It was worth noting that the CO_2 desorption capacities of diamine non-aqueous absorbents with different regulators were close to that of the 30M/P system, possibly owing to the fact that DEA, MDEA and TEA were alkanolamines with steric hindrance effects, and their reaction with CO_2 might produce lower stability carbamates and protonated amines which could be more easily regenerated.[47] Therefore, although the CO_2 absorption capacities of these diamine non-aqueous absorbents showed various reductions compared to 30M/P, their CO_2 desorption capacities were all at a high level.

CO_2 desorption efficiency was considered as an important parameter for evaluating the regeneration performance of non-aqueous absorbent systems. Based on the experiments described above, the CO_2 desorption efficiency curve of non-aqueous absorbents was plotted. The results showed that the CO_2 desorption efficiencies of non-aqueous absorbents with regulators were significantly higher compared to the 30M/P absorbent. Among them, the 25M5M/P system showed the best CO_2 desorption performance and its CO_2 desorption efficiency could reach 70.0%. MDEA was a tertiary amine with low reactivity towards CO_2. But it might have an interaction reaction with MEA to provide $MDEAH^+$ with lower energy barriers, thereby enabling the diamine non-aqueous absorbent with MDEA regulation to exhibit better regeneration capability. Accordingly, MDEA was considered the optimal regulator for MEA/PEG200 non-aqueous absorbent. Therefore, the MEA/MDEA/PEG200 non-aqueous absorbent was selected for further investigation.

3.2 CO_2 absorption performance

After identifying the excellent regulatory performance of MDEA, the effect of different MEA to MDEA ratios on CO_2

absorption and desorption performance of the absorbent were further investigated. The proportion of MDEA in diamine nonaqueous adsorbents was increased to 15 wt% to obtain an optimal adsorbent composition. The CO_2 absorbents prepared for the experiments are listed in Table S1.†

Firstly, the CO_2 absorption performance of MEA/MDEA/PEG200 solutions with different ratios was investigated, and the results are shown in Fig. 3. It could be seen that the CO_2 absorption rates of all the non-aqueous absorbents gradually decreased as the reaction proceeded, while their CO_2 absorption capacities increased and then tended to stabilize until the solutions were saturated. When there was no MDEA regulation, the MEA/PEG200 solution had the highest CO_2 absorption capacity, but the solution was accompanied by insoluble product generation. As the MDEA mass fraction increased, the CO_2 absorption capacity and absorption rate of MEA/MDEA/PEG200 solution both gradually decreased. It was due to the total amine concentrations of non-aqueous absorbents being 30 wt%, and the increased MDEA would lead to a decrease in MEA, which limited their CO_2 absorption capacity and absorption rate. In addition, as indicated in Table S2,† due to the relatively high viscosity of MDEA, the viscosity of MEA/MDEA/PEG200 solution increased obviously when the MDEA proportion was increased. It was not conductive to gas–liquid mass transfer, resulting in the reduction of CO_2 absorption capacity.

3.3 CO_2 desorption performance

3.3.1 Selection of MEA/MDEA/PEG200 concentration. In order to select the optimal solvent ratio, the CO_2 desorption performance of diamine non-aqueous absorbents with different MEA and MDEA mass fractions were further investigated at 373 K, and the results are shown in Fig. 4.

Fig. 4(a) exhibits the CO_2 desorption rate of MEA/MDEA/PEG200 solutions varied with time. As the solutions were heated from 313 K to the pre-set desorption temperature, the CO_2 desorption rates of all the diamine non-aqueous absorbents increased significantly within 0–13.3 min and reached their maximum values. After that, due to the rapid reduction of CO_2 amount in CO_2-rich solutions, the CO_2

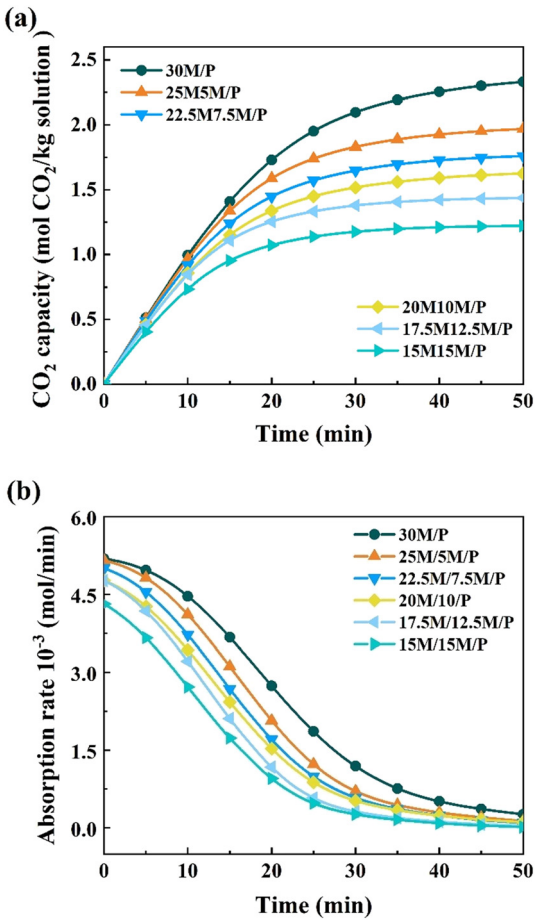

Fig. 3 Comparison of different mass fractions of MEA and MDEA in PEG200 solution for CO_2 absorption performance. (a) CO_2 absorption capacity; (b) CO_2 absorption rate (V_L = 0.05 kg, C_{total} = 30 wt%, $T_{absorption}$ = 313 K).

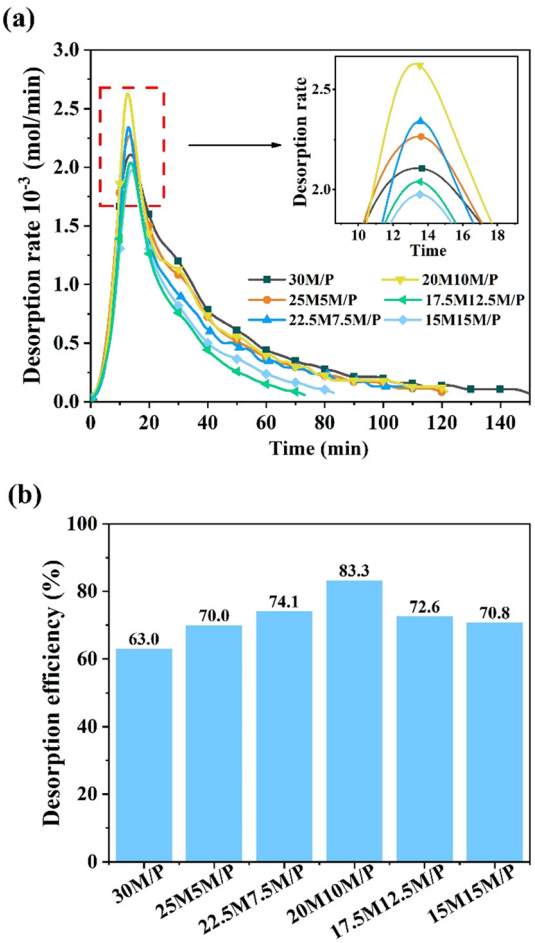

Fig. 4 Comparison of different mass fractions of MEA and MDEA in PEG200 solution for regeneration performance. (a) CO_2 desorption rate; (b) CO_2 desorption efficiency (V_L = 0.05 kg, C_{total} = 30 wt%, $T_{desorption}$ = 373 K).

desorption rates gradually decreased from 13.3 min until the regeneration process was completed. It was worth noting that the maximum CO_2 desorption rates of non-aqueous absorbents gradually increased with MDEA increasing from 0 to 10 wt%. It could be understood that MDEA as a tertiary alkanolamine participated in the reaction of MEA with CO_2 and produced more $MDEAH^+$ with relatively lower thermal stability. And $MDEAH^+$ could be easily desorbed during the regeneration process, thus the maximum CO_2 desorption rate of MEA/MDEA/PEG200 solution was significantly improved. Meanwhile, all MEA/MDEA/PEG200 solutions with different MEA to MDEA ratios took obviously shorter time to complete CO_2 desorption than MEA/PEG200 solution at the same desorption temperature. It would contribute to reducing energy consumption in absorbent regeneration processes. When the MDEA mass fraction was further increased from 10 wt% to 15 wt%, the maximum CO_2 desorption rates of MEA/MDEA/PEG200 absorbents with different solvent ratios began to decrease. It was explained that the CO_2 saturated absorption capacity of the MEA/MDEA/PEG200 absorbent decreased gradually with increasing proportion of MDEA, which resulted in a weaker CO_2 desorption driving force and a lower maximum CO_2 desorption rate. In contrast, the 20M10M/P solution exhibited relatively better regeneration performance during the first 13.3 min. The maximum CO_2 desorption rate of 20M10M/P solution could reach 2.61 × 10^{-3} mol min^{-1}, which was nearly 22% higher than that of 30M/P solution.

Apart from that, the CO_2 desorption efficiencies of all the non-aqueous absorbents were calculated according to eqn (5). As illustrated in Fig. 4(b), the CO_2 desorption efficiencies of diamine non-aqueous solutions based on MDEA regulation were significantly improved in comparison with that of MEA/PEG200 solution. In particular, the CO_2 desorption efficiency of 20M10M/P solution could reach 83.3%, which was about 32% higher than that of 30M/P solution. And it was 2.3 times higher than 30 wt% MEA non-aqueous solutions reported in relevant literature studies.[48,49] Likewise, 20M10M/P solution showed high CO_2 capture performance. The CO_2 absorption and desorption capacity of 20M10M/P solution could reach 1.62 mol kg^{-1} and 1.35 mol kg^{-1}, respectively. In conclusion, in order to ensure a relatively higher absorption capacity and better regeneration performance of the non-aqueous absorbent, 20 wt% MEA + 10 wt% MDEA + 70 wt% PEG200 was selected as the best composition for this work.

3.3.2 Cyclic absorption and desorption performance. Based on the above experiments, it was concluded that 20M10M/P was considered as the best solvent proportion in this work due to its excellent regeneration performance. Therefore, to further investigate the cycling stability of 20M10M/P solution, the effect of desorption temperature and time on CO_2 desorption efficiency of the non-aqueous absorbent was first investigated. As seen from Fig. 5(a), the maximum CO_2 desorption rate of 20M10M/P solution increased with regeneration temperature. Among them, the maximum CO_2 desorption rate could reach 4.13 × 10^{-3} mol min^{-1} at 393 K, which was 2.6 times higher than the maximum desorption rate at 363 K. And 20M10M/P solution completed desorption at 393 K in 67 min, which was shorter than that at other regeneration temperatures.

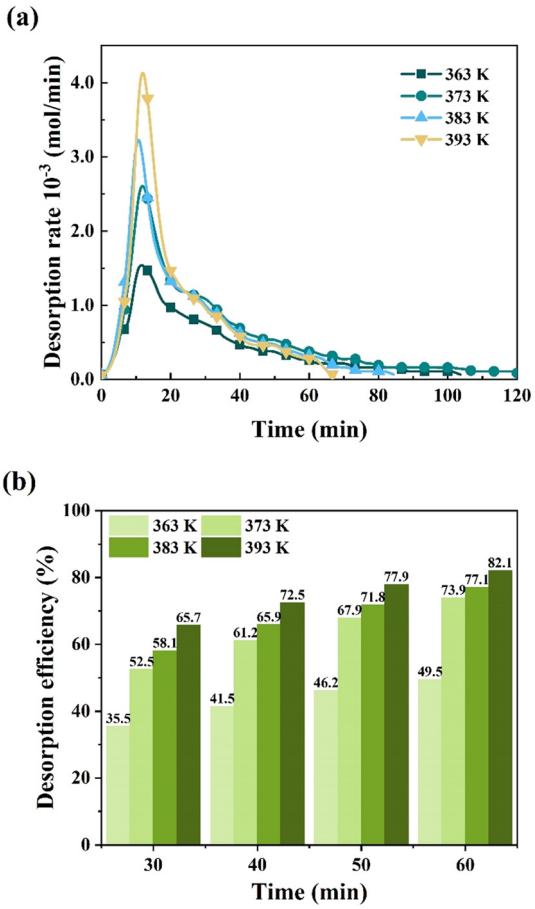

Fig. 5 Desorption performance of the 20M10M/P system at different temperatures. (a) CO_2 desorption rate; (b) CO_2 desorption efficiency (V_L = 0.05 kg, C_{MEA} = 20 wt%, C_{MDEA} = 10 wt%, C_{PEG200} = 70 wt%).

Furthermore, the effect of desorption temperature and time on CO_2 desorption efficiency was investigated and the results are shown in Fig. 5(b). It could be noticed that the CO_2 desorption efficiency increased significantly with the increase of desorption temperature in the same desorption time period. It was due to the fact that the absorbent regeneration process was an endothermic reaction, and the increased desorption temperature would shift the chemical equilibrium thus facilitating CO_2 release from the CO_2-rich solution. And the CO_2 desorption efficiency of 20M10M/P increased significantly with the increase of desorption time at the same desorption temperature. When the desorption time was 60 min, the CO_2 desorption efficiency of 20M10M/P solution could reach 82.1% at 393 K. In practical engineering applications, a faster CO_2 desorption rate, higher desorption efficiency and shorter desorption time would be beneficial to reduce the desorption tower volume, which could reduce CO_2 absorbent consumption. Therefore, in subsequent experiments to study the stability of the 20M10M/P system,

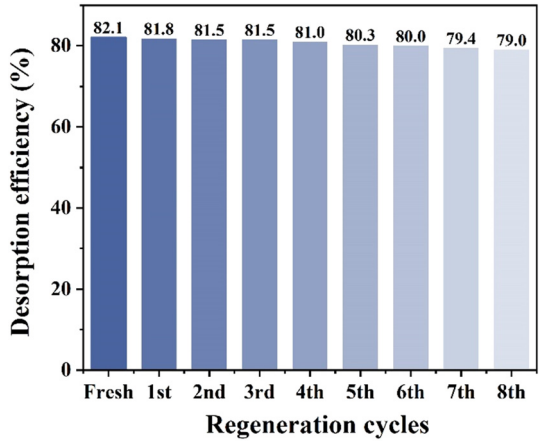

Fig. 6 Cyclic desorption efficiency of the MEA/MDEA/PEG200 system (V_L = 0.05 kg, C_{MEA} = 20 wt%, C_{MDEA} = 10 wt%, C_{PEG200} = 70 wt%, $T_{absorption}$ = 313 K, $T_{desorption}$ = 393 K).

60 min and 393 K were selected as the best experimental conditions for cyclic regeneration.

As shown in Fig. 6, the long-term stability of the 20M10M/P absorbent was tested in 8-cycles of absorption–desorption experiments. It could be noticed that the CO_2 desorption efficiency of the 20M10M/P system decreased slightly with cycle number, but the overall desorption efficiency was as high as 79%. As a result, the 20M10M/P absorbent had a clear advantage in recycling for CO_2 capture due to its better stability.

3.4 Regeneration heat duty

Based on the comprehensive analysis of CO_2 absorption and desorption experiments described above, 20M10M/P was considered to be the optimal diamine non-aqueous absorbent in this work. In order to evaluate the energy-saving potential of the 20M10M/P system compared to 30M/H_2O and 30M/P systems, their regeneration heat duties were calculated respectively, and the results are illustrated in Fig. 7 (the CO_2 absorption and desorption performances of 30 wt% MEA aqueous solutions are detailed in Fig. S4†).

Firstly, the VLE data of 30M/H_2O, 30M/P and 20M10M/P systems were measured over CO_2 partial pressures between 3.1 and 14.9 kPa at different absorption temperatures. Then, according to the VLE curves shown in Fig. S3,† CO_2 desorption reaction heat could be calculated using eqn (9). The linear fitting results showed that the slope of the $\ln P_{CO_2}$ and $1/T$ curve for 30M/H_2O was −9631.0 K, which corresponded to desorption reaction heat as high as 1.82 GJ per ton CO_2. The slopes of $\ln P_{CO_2}$ and $1/T$ curves for 30M/P and 20M10M/P were −9314.4 and −7409.3 K, corresponding to desorption reaction heats of 1.76 GJ per ton CO_2 and 1.40 GJ per ton CO_2, respectively. It could be seen that the desorption reaction heat of the 20M10M/P system was significantly lower than that of 30M/H_2O and 30M/P systems. This phenomenon might be related to the products generated

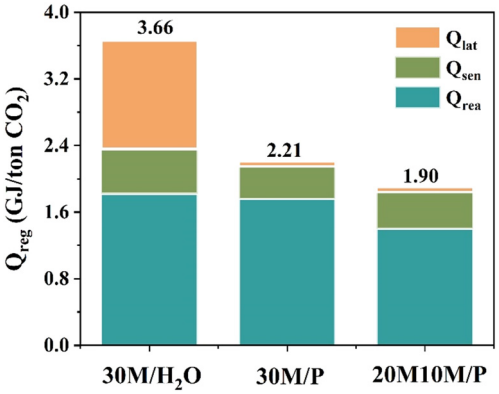

Fig. 7 Regeneration heat duty of different absorbent systems at 393 K.

in the above absorbents. To regenerate the absorbent, it was required to supply heat to release CO_2 from CO_2 absorption products such as carbamate and carbonate/bicarbonate. In addition, it was also necessary to provide heat for the deprotonation of protonated amines. Since MEA was used as the main CO_2 absorbent in these systems, they all produced the same carbamate. But for the 30M/P system, the terminal hydroxyl groups in PEG200 molecules could form strong hydrogen bonds, which would enhance the formation of weakly adsorbed CO_2 in the presence of amine groups. In view of this, the 30M/P system would have higher CO_2 desorption efficiency and desorption reaction heat compared to 30M/H_2O under the same regeneration conditions. Likewise, the introduction of MDEA probably changed the type of protonated amine, resulting in the generation of $MDEAH^+$, which was easier to regenerate compared to protonated MEA ($MEAH^+$). For these reasons, the 20M10M/P system had the lowest desorption reaction heat.

The sensible heat was the energy required to heat the solution from absorption temperature to desorption temperature, which was related to the specific heat capacity of the solution. According to eqn (10)–(12), the sensible heat of 30M/H_2O, 30M/P and 20M10M/P systems could be calculated, and they were 0.54, 0.39, and 0.44 GJ per ton CO_2, respectively. As the specific heat capacity of organic solvents was obviously lower than that of water, the sensible heat of non-aqueous absorbents was lower than that of MEA aqueous solution.

During the CO_2 desorption process, the evaporation latent heat was the energy required for the phase change of the absorbent, and mainly depended on its evaporation enthalpy. Due to the high boiling point and low vapor pressure of PEG200, both 30M/P and 20M10M/P systems showed lower evaporative loss of solvent during regeneration, resulting in their lower evaporation latent heat values.

According to the above thermodynamic analysis, the total regeneration heat duty for the 20M10M/P system was 1.9 GJ per ton CO_2, which was 48.1% lower than that of the 30M/H_2O system. In particular, the desorption reaction heat of the 20M10M/P system was reduced by 20% compared to the 30M/P system. This indicated that the addition of MDEA

could effectively change the thermal stability of CO_2 absorption products of the 30M/P absorbent, thus realizing a lower energy consumption for the absorbent regeneration. On the whole, the 20M10M/P system showed high CO_2 absorption capacity, high CO_2 desorption efficiency and low regeneration energy consumption, which made it a promising alternative absorbent for energy-efficient CO_2 capture.

3.5 Reaction mechanism of CO_2 capture

3.5.1 FT-IR and ^{13}C NMR analysis. In order to elucidate the reaction mechanisms between non-aqueous absorbents and CO_2, FT-IR analysis was used to investigate the substance composition of 30M/P and 20M10M/P systems before and after CO_2 absorption as well as after CO_2 desorption. As shown in Fig. 8(a), it showed that after CO_2 absorption by 30M/P solution, a new vibrational peak appeared at 1314 cm^{-1}, and the peak of $-NH_2$ at 2923 cm^{-1} was significantly weaker compared to peaks before CO_2 absorption. It indicated the formation of a carbamate group ($-NHCOO^-$).

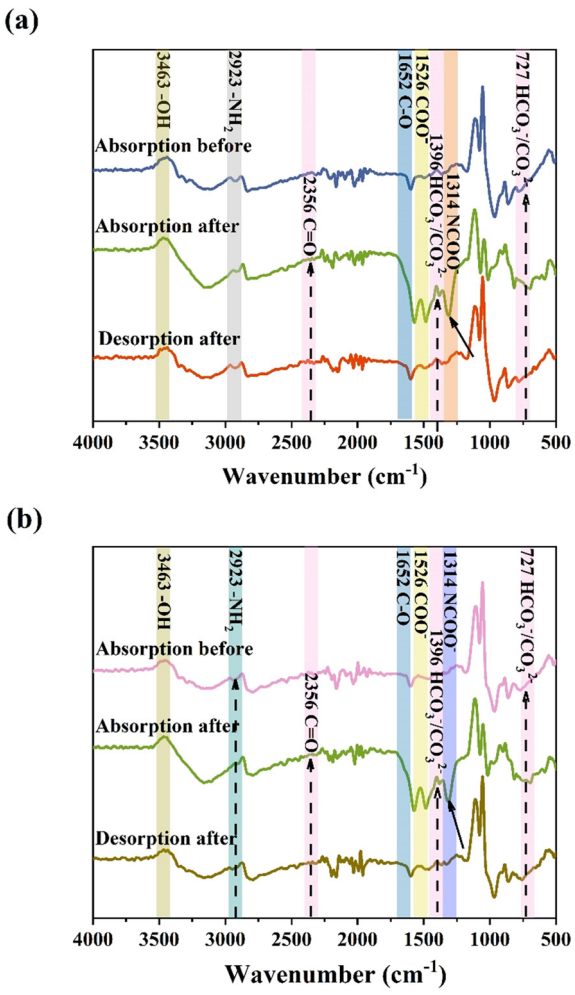

Fig. 8 FT-IR spectra for (a) 30M/P and (b) 20M10M/PEG200 systems.

The peaks at 1526 cm^{-1} and 1652 cm^{-1} were attributed to the asymmetric stretching of COO^- and the carbonyl stretching of carbamic acid. Moreover, 30M/P solution also showed peaks at 727, 1396 and 2356 cm^{-1} generated by C–O and C═O stretching vibrations. And it was noticed that the peak of –OH in PEG200 at 3463 cm^{-1} diminished after CO_2 absorption. It was speculated that HCO_3^-/CO_3^{2-} was generated after PEG200 reacted with CO_2.[50] When 30M/P solution was regenerated after CO_2 absorption, it was shown that the peak of $NCOO^-$ at 1314 cm^{-1} gradually weakened in the IR spectrum, but the peak of $-NH_2$ at 2923 cm^{-1} did not have more obvious changes compared with that after CO_2 absorption, which indicated that $MEAH^+$ produced by 30M/P after CO_2 absorption was not sufficiently decomposed.

For the 20M10M/P system, FT-IR tests indicated that IR spectra showed similar $NCOO^-$ and HCO_3^-/CO_3^{2-} characteristic peaks at 1314, 727, 1396 and 2356 cm^{-1} after CO_2 absorption. But different from the 30M/P system, HCO_3^-/CO_3^{2-} in the 20M10M/P system could be produced not only by reaction of –OH with CO_2 in PEG200, but also by reaction of –OH with CO_2 in MDEA.[51] MDEA addition resulted in more decomposable carbonates or bicarbonates in solution, which might be the reason for the higher desorption efficiency of 20M10M/P solution than 30M/P solution. In addition, the characteristic peaks of HCO_3^-/CO_3^{2-} and carbamate in 20M10M/P solution almost disappeared in the IR spectrum after CO_2 desorption, and the $-NH_2$ peak at 2923 cm^{-1} was also significantly changed to its status before CO_2 absorption. According to zwitterion theory, the amino group of MDEA in non-aqueous absorbents could not react directly with CO_2. Therefore, it might be that zwitterions generated by the reaction between MEA and CO_2 interacted with MDEA to produce $MDEAH^+$, which had a lower energy barrier than $MEAH^+$ and thus was more prone to decomposition at high temperature. To summarize, CO_2 absorption products in the 20M10M/P system could be desorbed more adequately and with higher CO_2 desorption efficiency.

To further investigate the C-containing substance distribution after CO_2 capture by non-aqueous absorbents, ^{13}C-NMR characterization was used to analyze substance composition changes of 30M/P and 20M10M/P systems before and after CO_2 absorption as well as after CO_2 desorption. It could be seen in Fig. 9(a) that new peaks appear at 159.5 cm^{-1} and 164.6 cm^{-1} after 30M/P absorbent CO_2 absorption, which corresponded to HCO_3^-/CO_3^{2-} and $NCOO^-$, respectively. And the $-CH_2-NH_2$ group characteristic peak at 41.6 cm^{-1} was significantly weaker than that before CO_2 absorption, which confirmed carbamate formation in 30M/P solution. In addition, the characteristic peak at 48.2 cm^{-1} was attributed to carbon in $MEAH^+$, and the $MEAH^+$ peak was significantly weakened after CO_2 absorption, which indicated $MEAH^+$ production. The carbon signals of –NCOO– and HCO_3^-/CO_3^{2-} at 159.9 cm^{-1} and 164.6 cm^{-1} were found to disappear after CO_2-rich solution desorption, but the peak of $-CH_2-NH-$ at 41.6 cm^{-1} was not restored to its pre-CO_2

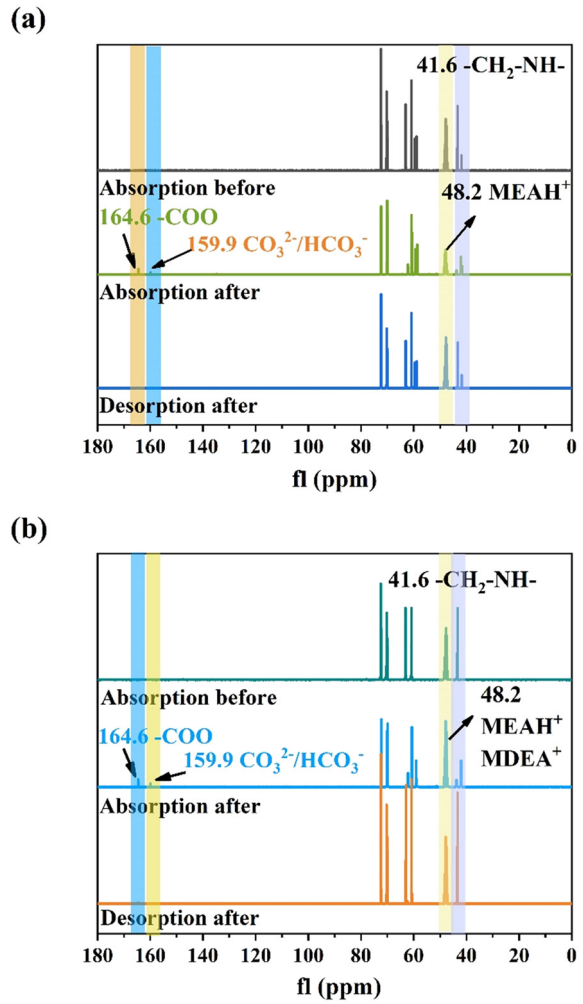

Fig. 9 ^{13}C-NMR spectra for (a) 30M/P and (b) 20M10M/PEG200 systems.

absorption status. It indicated that 30M/P rich solution desorption was not satisfactory and the absorption products were not completely regenerated.

The ^{13}C-NMR spectrum of 20M10M/P solution is shown in Fig. 9(b), and the carbon signal peaks at 41.6, 159.9 and 164.6 cm^{-1} after CO_2 absorption remained consistent with those corresponding to 30M/P. But it could be noticed that the characteristic peak at 48.2 cm^{-1} was significantly enhanced compared to that before CO_2 absorption. It might be due to the fact that $MEAH^+$ had a relatively higher energy barrier, and thus zwitterions produced by interaction of MEA with CO_2 were more prone to interact with MDEA, which produced a lower energy $MDEAH^+$. After CO_2 desorption of 20M10M/P solution, it was found that although $NCOO^-$ and HCO_3^-/CO_3^{2-} peaks disappeared, carbon signal peaks of $-CH_2-NH-$ and $MDEAH^+$ were also restored to their status before CO_2 absorption. It indicated that in comparison to the 30M/P system, the CO_2 absorption products of the 20M10M/P system were more accessible for desorption. It might be related to the stability of absorption products, in which $MDEAH^+$ had a lower stability than $MEAH^+$ due to the steric hindrance effect and therefore could be regenerated more efficiently under the same CO_2 desorption conditions.

3.5.2 Calculation of the reaction pathways. To further investigate the regulatory effect of MDEA in the non-aqueous absorbent MEA/PEG200, the interaction energy and activation energy potential of the 20M10M/P system reacting with CO_2 were calculated. Based on FT-IR and ^{13}C-NMR tests, the non-aqueous absorbent 20M10M/P reacted with CO_2 through $-NH_2$ and –OH groups to produce carbamate and HCO_3^-/CO_3^{2-}, respectively. Therefore, the reaction pathways and energies were predicted separately for three different transient reactions, as shown in Fig. 10(a). Among them, TS1 corresponds to $-NH_2$ reacting with CO_2 (pathway 1); TS2 corresponds to –OH reacting with CO_2 in MDEA (pathway 2); TS3 corresponds to –OH reacting with CO_2 in PEG200 (pathway 3). As illustrated in Fig. 10(a), the activation energy barriers calculated in this paper for the three different reaction paths of the 20M10M/P absorbent with CO_2 were similar to reported studies.[52] In particular, TS1 showed the smallest energy barrier, indicating that the $-NH_2$ of MEA reacting with CO_2 to produce carbamate played a dominant

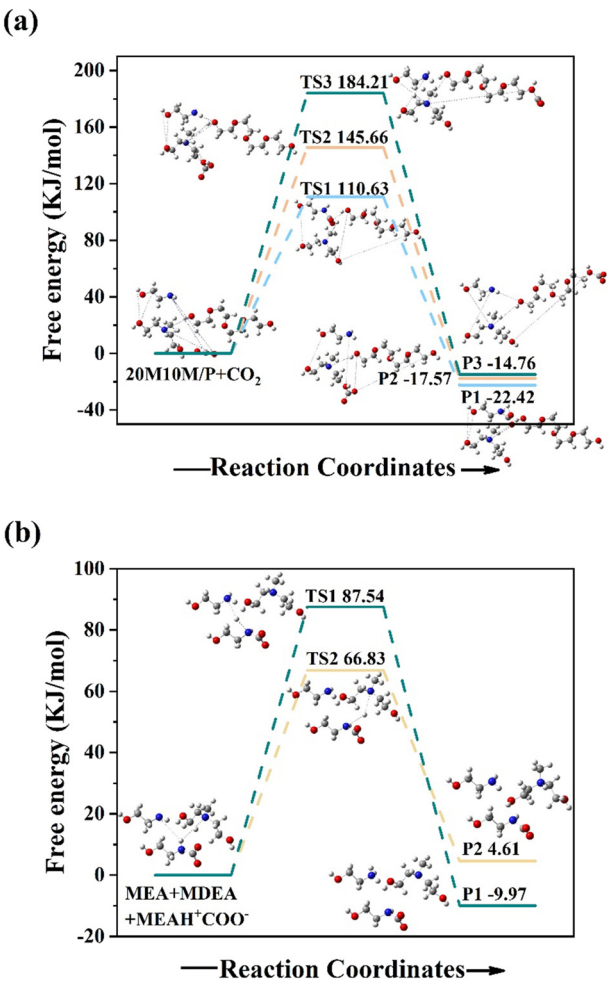

Fig. 10 Activation energy barrier and reaction energy calculations for (a) 20M10M/P system with CO_2 and (b) MDEA and MEA with $MEAH^+$, respectively.

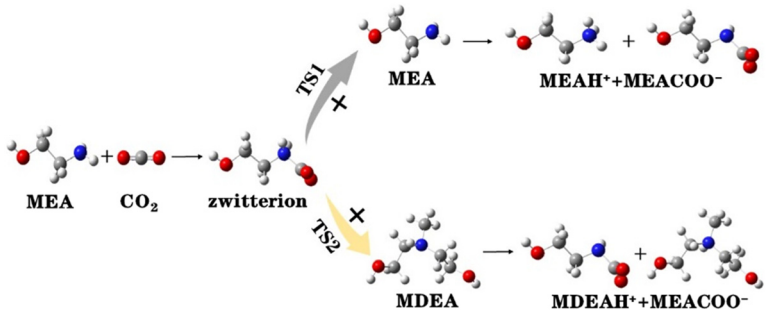

Fig. 11 The proposed mechanism of 20M10M/P system CO_2 absorption.

role in the 20M10M/P absorbent. In the reaction of the –OH group with CO_2, the activation energy barrier of reaction through the –OH group in MDEA with CO_2 was obviously lower than that in PEG200, which showed that the ability of –OH in MDEA to react with CO_2 was relatively greater.

In addition, for clarifying the regulatory effects of MDEA, the activation energies of zwitterions reacting with MEA and MDEA were investigated, respectively. It could be seen from Fig. 10(b) that the TS1 path activation energy potential for zwitterions reacting with MEA to produce $MEAH^+$ was 87.54 kJ mol^{-1}, while the TS2 path activation energy for reacting with MDEA to produce $MDEAH^+$ was 66.86 kJ mol^{-1}. It indicated that zwitterions reacted with MDEA more strongly than with MEA in the 20M10M/P absorbent. It also demonstrated that $MDEAH^+$ had lower energy barriers and was more easily regenerated during the desorption process. Therefore, the MEA/PEG200 solution with MDEA regulation resulted in a higher desorption efficiency, which was consistent with experimental results (Fig. 11).

4. Conclusions

In this study, a novel non-aqueous diamine absorbent based on alkanolamine regulation was proposed for CO_2 capture. In the non-aqueous absorbent system, MEA as the main absorbent guaranteed a high CO_2 absorption capacity and absorption rate, MDEA as the regulator provided a reaction pathway with a low activation energy barrier, and PEG200 was used as a cosolvent due to its low evaporation enthalpy and non-toxicity. When the total amine concentration was 30 wt%, among which the concentrations of MEA and MDEA were 20 wt% and 10 wt%, the CO_2 absorption capacity and maximum desorption efficiency reached 1.62 mol kg^{-1} and 82.1%. After 8 regenerations, the CO_2 desorption efficiency of the non-aqueous absorbent 20M10M/P could still reach 79%. The total regeneration heat duty of the 20M10M/P system was 1.90 GJ per ton CO_2, which was 48.1% lower than that of 30 wt% MEA aqueous solution. And its desorption reaction heat was reduced by 20% compared to the 30M/P system. FT-IR, ^{13}C-NMR tests and DFT calculations showed that protonated MEA generated by the reaction between MEA and CO_2 was not adequately regenerated at high temperature due to its high activation energy barrier. But the addition of MDEA would change the species of protonated amine in the non-aqueous absorbent, generating more $MDEAH^+$ with a lower energy barrier and resulting in easier regeneration. Thus, the desorption reaction heat of the 20M10M/P system was significantly reduced. In conclusion, this study established a groundwork for the development of non-aqueous absorbents as an effective way for low-energy CO_2 capture.

Conflicts of interest

There are no conflicts to declare.

Acknowledgements

This work was supported by the National Natural Science Foundation of China (Grants 52271356) and Guangdong Province Natural Resources Project (2022-32).

References

1 Z. Liu, Z. Deng, S. J. Davis, C. Giron and P. Ciais, *Nat. Rev. Earth Environ.*, 2022, **3**, 217–219.
2 K. Zickfeld, D. Azevedo, S. Mathesius and H. Matthews, *Nat. Clim. Change*, 2021, **11**, 613–617.
3 T. Borhani and M. Wang, *Renewable Sustainable Energy Rev.*, 2019, **114**, 109299.
4 F. Vega, F. Baena-Moreno, L. Gallego Fernández, E. Portillo, B. Navarrete and Z. Zhang, *Appl. Energy*, 2020, **260**, 114313.
5 X. Zhu, H. Lu, K. Wu, Y. Zhu, Y. Liu, C. Liu and B. Liang, *Environ. Sci. Technol.*, 2020, **54**, 7570–7578.
6 Y. Shen, J. Chen, H. Wang, S. Zhang, C. Jiang, J. Ye, L. Wang and J. Chen, *Appl. Energy*, 2020, **260**, 114343.
7 S. Zheng, M. Tao, Q. Liu, L. Ning, Y. He and Y. Shi, *Environ. Sci. Technol.*, 2014, **48**, 8905–8910.
8 Z. Liang, W. Rongwong, H. Liu, K. Fu, H. Gao, F. Cao, R. Zhang, T. Sema, A. Henni, K. Z. Sumon, D. Nath, D. Gelowitz, W. Srisang, C. Saiwan, A. Benamor, M. J. Al-Marri, H. Shi, T. Supap, C. W. Chan, Q. Zhou, M. R. Abu-Zahra, M. Wilson, W. Olson, R. O. Idem and P. Tontiwachwuthikul, *Int. J. Greenhouse Gas Control*, 2015, **40**, 26–54.
9 R. Zhang, X. Zhang, Q. Yang, H. Yu, Z. Liang and X. Luo, *Appl. Energy*, 2017, **205**, 1002–1011.
10 W. M. Budzianowski, *Int. J. Greenhouse Gas Control*, 2016, **49**, 108–120.

11 S. Zhang, Y. Shen, P. Shao, J. Chen and L. Wang, *Environ. Sci. Technol.*, 2018, **52**, 3660–3668.
12 K. Maneeintr, R. O. Idem, P. Tontiwachwuthikul and A. G. H. Wee, *Ind. Eng. Chem. Res.*, 2010, **49**, 2857–2863.
13 X. Zhang, G. Jing, B. LV, F. Liu and Z. Zhou, *Appl. Energy*, 2019, **235**, 379–390.
14 X. Zhang, X. Zhang, H. Dong, Z. Zhao, S. Zhang and Y. Huang, *Energy Environ. Sci.*, 2012, **5**, 6668–6681.
15 K. Zhu, H. Liu, C. Liu, K. Wu, W. Jiang, J. Cheng, S. Tang, H. Yue, Y. Liu and B. Liang, *Ind. Eng. Chem. Res.*, 2019, **58**, 3811–3821.
16 L. Bihong, Y. Kexuan, Z. Xiaobin, Z. Zuo-ming and G. H. Jing, *Appl. Energy*, 2020, **264**, 114703.
17 E. Torralba-Calleja, J. B. Skinner and D. Gutiérrez-Tauste, *J. Chem.*, 2013, 1–16.
18 M. S. Shannon, M. S. Hindman, S. P. Danielsen, J. M. Tedstone, R. D. Gilmore and J. E. Bara, *Sci. China: Chem.*, 2012, **55**, 1638–1647.
19 X. Liu, G. Zhou, S. Zhang and X. Yao, *Fluid Phase Equilib.*, 2009, **284**, 44–49.
20 B. E. Gurkan, B. F. Goodrich, E. M. Mindrup, L. E. Ficke, M. Massel, S. Seo, T. P. Senftle, H. Y. Wu, M. Glaser, J. K. Shah, E. J. Maginn, J. F. Brennecke and W. F. Schneider, *J. Phys. Chem. Lett.*, 2010, **1**, 3494–3499.
21 H. Kierzkowska-Pawlak and K. Sobala, *Int. J. Greenhouse Gas Control*, 2020, **100**, 103102.
22 X. Zhou, C. Liu, J. Zhang, Y. Fan, Y. Zhou, L. Zhang, S. Tang, S. Mo, H. Zhu and Z. Zhu, *Energy*, 2023, **270**, 126930.
23 L. Bai, S. Lu, Q. Zhao, L. Chen, Y. Jiang, C. Jia and S. Chen, *SSRN Electronic Journal*, 2022, **450**, 138490.
24 H. Hu, M. Fang, F. F. Liu, T. Wang, Z. Xia, W. Zhang, C. Ge and J. Yuan, *Appl. Energy*, 2022, **324**, 119570.
25 Y. Shen, C. Jiang, S. Zhang, J. Chen, L. Wang and J. Chen, *Appl. Energy*, 2018, **230**, 726–733.
26 A. Shamiri, M. S. Shafeeyan, H. Tee, C. Leo, M. K. Aroua and N. Aghamohammadi, *J. Nat. Gas Sci. Eng.*, 2016, **35**, 605–613.
27 U. Shoukat, E. Baumeister, D. D. Pinto and H. K. Knuutila, *J. Nat. Gas Sci. Eng.*, 2019, **62**, 26–37.
28 O. Aschenbrenner and P. Styring, *Energy Environ. Sci.*, 2010, **3**, 1106–1113.
29 J. Li, C. You, L. Chen, Y. Ye, Z. Qi and K. Sundmacher, *Ind. Eng. Chem. Res.*, 2012, **51**, 12081–12088.
30 F. Bougie, D. Pokras and X. Fan, *Int. J. Greenhouse Gas Control*, 2019, **86**, 34–42.
31 H. Guo, H. Li and S. Shen, *Energy Fuels*, 2018, **32**, 6943–6954.
32 J. Li, L. Chen, Y. Ye and Z. Qi, *J. Chem. Eng. Data*, 2014, **59**, 1781–1787.
33 Y. Yu, H. F. Lu, T. T. Zhang, Z. X. Zhang, G. X. Wang and V. Rudolph, *Ind. Eng. Chem. Res.*, 2013, **52**, 12622–12634.
34 H. Guo, C. Li, X. Shi, H. Li and S. Shen, *Appl. Energy*, 2019, **239**, 725–734.
35 Z. Tan, S. Zhang, X. Yue, F. Zhao, F. Xi, D. Yan, H. Ling, R. Zhang, F. Tang, K. You, H. Luo and X. Zhang, *Sep. Purif. Technol.*, 2022, **298**, 121577.
36 J. Crooks and J. Donnellan, *J. Chem. Soc., Perkin Trans. 1*, 1989, **4**, 331–333.
37 S. Laddha and P. Danckwerts, *Chem. Eng. Sci.*, 1981, **3**, 479–482.
38 P. V. Kortunov, M. Siskin, L. Baugh and D. C. Calabro, *Energy Fuels*, 2015, **29**, 5940–5966.
39 T. Ping, Y. Dong and S. Shen, *ACS Sustainable Chem. Eng.*, 2020, **8**, 18071–18082.
40 S. Liu, H. Gao, C. He and Z. Liang, *Appl. Energy*, 2019, 233–234.
41 X. Zhou, G. Jing, B. Lv, F. Liu and Z. Zhou, *Appl. Energy*, 2019, **235**, 379–390.
42 M. Ma, Y. Liu, Y. Chen, G. Jing, B. Lv, Z. Zhou and S. Zhang, *J. CO2 Util.*, 2023, **67**, 102277.
43 H. Shi, A. Naami, R. Idem and P. Tontiwachwuthikul, *Int. J. Greenhouse Gas Control*, 2014, **26**, 39–50.
44 X. Zhang, R. Zhang, H. Liu, H. Gao and Z. Liang, *Appl. Energy*, 2018, **218**, 417–429.
45 V. Wiesmet, E. Weidner, S. Behme, G. Sadowski and W. Arlt, *J. Supercrit. Fluids*, 2000, **17**, 1–12.
46 Y. Li, J. Gao, J. Li, Y. Li, M. T. Bernards, M. Tao, Y. He, Y. He and Y. Shi, *Energy Fuels*, 2020, **34**, 11270–11281.
47 H. Svensson, V. Z. Velasco and C. Hulteberg, *Int. J. Greenhouse Gas Control*, 2014, **30**, 1–8.
48 B. Wang, X. Chen and G. Yu, *Ind. Eng. Chem. Res.*, 2021, **60**, 3871–3880.
49 B. Wang, X. Chen and G. Yu, *Sep. Purif. Technol.*, 2022, **294**, 121173.
50 W. Qian, J. Hao, M. Zhu, P. Sun, K. Zhang, X. Wang and X. Xu, *J. CO2 Util.*, 2022, **59**, 101955.
51 N. Ahmad, X. Wang, P. Sun, Y. Chen, F. Rehman, J. Xu and X. Xu, *Renewable Energy*, 2021, **177**, 23–33.
52 B. Cao, J. Du, S. Liu, X. Zhu, X. Sun, H. Sun and H. Fu, *RSC Adv.*, 2016, **6**, 10462–10470.